
Separation and Preconcentration of Anionic Dyes Using Magnetic Nanoparticles with Modify Polymer Ionic Liquid

Mahboobeh Falahati, Majid Soleimani, Fateme Aflatouni*

Department of Chemistry, Imam Khomeini International University (IKIU), Qazvin, Iran

Email address:

mahboobefalahati1375@gmail.com (Mahboobeh Falahati), m-soleimani@hotmail.com (Majid Soleimani),

Fatemeaflatouni@yahoo.com (Fateme Aflatouni)

*Corresponding author

To cite this article:

Mahboobeh Falahati, Majid Soleimani, Fateme Aflatouni. Separation and Preconcentration of Anionic Dyes Using Magnetic Nanoparticles with Modify Polymer Ionic Liquid. *American Journal of Heterocyclic Chemistry*. Vol. 9, No. 1, 2023, pp. 1-8.

doi: 10.11648/j.ajhc.20230901.11

Received: January 22, 2023; **Accepted:** April 7, 2023; **Published:** April 20, 2023

Abstract: In this study, functionalized magnetic nanoparticles of poly (ionic liquid) 1-allyl-3-methylimidazolium chloride were prepared through free radical copolymerization method and tested as a high efficient adsorbent for the removal of anionic dyes in water samples. The physical and chemical structure of prepared magnetic nanoparticles (MNPs) were investigated using Fourier transform infrared spectroscopy (FT-IR), X-ray powder diffraction (XRD), transmission electron microscopy (TEM) and scanning electron microscopy (SEM). Next, synthesized magnetic nanoparticles were used in magnetic solid phase extraction (MSPE) method to extract three anionic dyes (Alizarin Red S, Congo Red and Methyl Orange) in water samples. Also, the effect of several parameters such as pH, temperature, contact time and amount of adsorbent was investigated and the optimum values were determined. In addition, the adsorbent has a high ability to remove anionic dyes from water samples containing different dyes. Limit of detection (LOD), limit of quantitation (LOQ), and correlation coefficient were determined for methyl orange, Congo red and alizarin red S dyes under optimum conditions. The synthesized magnetic nanoparticles can be collected by an external magnetic field and regenerated with an alkaline solution (NaOH) and reused. The obtained results showed that the MNPs@PIL method was very efficient and successful in removing dye pollutants in water samples.

Keywords: Poly (Ionic Liquid), Magnetic Solid-Phase Extraction (MSPE), Fe₃O₄, Nanoparticles, Alizarin Red S, Congo Red, Methyl Orange

1. Introduction

In recent years, solid phase extraction (SPE) has attracted considerable attention in the field of sample preparation and extraction [1]. The magnetic solid phase extraction (MSPE) method is known as an advanced method of solid phase extraction (SPE). In this method, the analytes are allowed to interact with the magnetic adsorbent for several minutes, and then the analytes are removed by an external magnetic field. The magnetic adsorbent property makes the separation process easier and reduces the extraction time [2]. However, NPs are easily oxidized by changing environmental conditions. Therefore, to prevent this phenomenon, NPs surface modification should be done [3]. In this regard, the hydrophobic silica nanoparticles have a strong ability to

interact with other functional groups, Silica not only protects the magnetic core but also prevents the direct contact of additional agents with the magnetic cores [4]. Today, ionic liquids have attracted wide attention because of their unique properties and applications. Most ionic liquids are in their liquid form at a temperature of less than 100°C, The composition of ionic liquids consists of bulky and asymmetric cations and low-volume anions [5]. Polymeric ionic liquids are a novel class of poly electrics materials derived by the polymerization of IL monomers [6]. PILs are used as a coating on the absorbent surface for extraction and preconcentration of different analytes [7-9]. The solid phase extraction based on polymeric ionic liquids can be used several times because polymeric ionic liquids enhance stability and durability [10].

Dyes have different uses in different industries such as

leather, plastic, food, etc. Azo dyes are widely used in textile and dyeing industries. Azo dyes are composed of one or more groups of organic aromatic compounds [11]. Most of the azo dyes are carcinogenic, mutagenic, and toxic [12], and the presence of these dyes in water creates serious problems for humans, living organisms, and the environment. MO is a water-soluble dye that is used in the dyeing and textile industries [13]. CR is carcinogenic to humans due to the presence of benzene rings [14]. ARS is a type of water-soluble dye and is part of complex aromatic compounds that are very durable and resistant to light and heat. This category of dyes can be removed from water samples using different methods and techniques such as surface adsorption, flocculation, and oxidation, among all these methods, surface adsorption is the most used. Determining the low concentration of dyes in water samples is a big problem, so it is necessary to use a precise technique for dye separation and preconcentration [15-18].

In this study, PIL was modified on the adsorbent surface through free radical polymerization. The new MNPs@PIL nanoparticles have a high ability to separate and preconcentrate the anionic dyes methyl orange, Congo red and alizarin red S with different concentrations. Also, the obtained MNPs@PIL nanocomposite was used 11 consecutive times to extract anionic dyes. Therefore, it has a high ability to remove anionic dyes from water samples.

2. Experimental

2.1. Materials and Apparatus

Iron (III) chloride hexahydrate ($FeCl_3 \cdot 6H_2O$) (99%), Iron (II) chloride tetrahydrate ($FeCl_2 \cdot 4H_2O$) (98%), Ammonia (NH_3 , 25%, W/W), methanol, ethanol, Chloroform, hydrochloric acid, Sodium hydroxide, Methyl orange (MO), Alizarin red (AR), and Congo Red (CR), vinyltriethoxysilane (VTES) and Tetra ethyl orthosilicate (TEOS) were purchased from Merck, 2,2'-Azobisisobutyronitrile (AIBN) was purchased from Acros and 1-Allyl-3-methylimidazolium chloride (98%) was purchased from Atlas chemical (Tehran, Iran).

The concentration of the samples were determined using a Camspec model UV-vis spectrophotometer. The morphologies of the MNPs@PIL were examined using scanning electron microscopy (SEM) instrument, and Transmission electron microscope (TEM) instrument. The Structure analysis of adsorbent was analyzed by X-ray diffractometer (XRD). To identify the organic compounds, inorganic compounds, and functional groups of the obtained product, a Bruker Tensor Fourier transform infrared spectrometer (FT-IR) was used. The pH measurements were carried out using a Metrohm pH meter (220L Neo Met, Korea).

2.2. Synthesis of $Fe_3O_4@SiO_2@PIL$

To prepare Fe_3O_4 nanoparticles, $FeCl_3 \cdot 6H_2O$ (5.2g) and $FeCl_2 \cdot 4H_2O$ (2.0g) were dissolved in 100 mL deionized

water. Then HCL 12mol/L and ammonia (25% (W/W)) were added to the solution. The obtained sediment was separated by a strong magnet. Preparation of Superparamagnetic nanoparticles with a thin layer of silica ($Fe_3O_4@SiO_2$) was performed through sol-gel polymerization method. Preparation of ($Fe_3O_4@SiO_2@VTES$) was performed via the reaction between $Fe_3O_4@SiO_2$ and vinyltriethoxysilane.

PIL was immobilized on the surface of magnetic nanoparticles by free radical copolymerization of 1-allyl-3-methylimidazolium chloride and ($Fe_3O_4@SiO_2@VTES$) using AIBN as an initiator. The obtained (MNPs@PIL) product was collected by an external magnetic field. Then they were dried under vacuum at 45°C [10].

2.3. Magnetic Solid phase Extraction Method (MSPE)

80 mg of prepared magnetic nanoparticles PIL adsorbent was weighted and transferred into a 25 ml beaker, then immersed in 20 ml of 0.1M sodium hydroxide solution for 24 hours to activate the imidazolium groups on the adsorbent surface. Then, in order to neutralize the adsorbent, it was washed several times with deionized water. For each MSPE procedure, 5 ml of the analyte with a certain concentration was added to the adsorbent. The mixture was stirred by a mechanical stirrer for 15 minutes, and finally, the adsorbent was separated by an external magnet.

3. Results and Discussion

3.1. Characterization of MNPs@PIL

3.1.1. FT-IR Spectra

The FT-IR spectra of Fe_3O_4 , $Fe_3O_4@SiO_2$, $Fe_3O_4@SiO_2@VTES$, and MNPs@PIL are shown in "Figure 1". In Fe_3O_4 FT-IR spectra the absorbance band at 3414 cm^{-1} is related to the stretching vibration of the O-H. In the $Fe_3O_4@SiO_2$ spectrum, the strong absorbance band at 1099 cm^{-1} can be ascribed to Si-O-Si stretching vibration. Moreover, the absorbance band at 3062 cm^{-1} and 2960 cm^{-1} shows the presence of $-CH_2$ and $-CH_3$ groups respectively, which corresponds to the spectrum of $Fe_3O_4@SiO_2@VTES$. In the spectrum of MNPs@PIL absorbance band at 1551 cm^{-1} and 1463 cm^{-1} indicates the existence of imidazolium rings on the surface of MNPs.

3.1.2. XRD Patterns

The XRD patterns of the Fe_3O_4 and MNPs@PIL are shown in "Figure 2", XRD patterns exhibited strong diffraction peaks at 30.1° , 35.9° , 37.1° , 43.2° , 54° , 57.3° , and 63° that have been appeared for both of them. The results showed that the crystal structure of Fe_3O_4 particles has not changed after modification with ionic poly liquid.

3.1.3. Scanning Electron Microscope (SEM)

The morphology of MNPs@PIL was investigated by SEM. SEM image in "Figure 3", reveals that the size of the particles is between 18-36 nm.

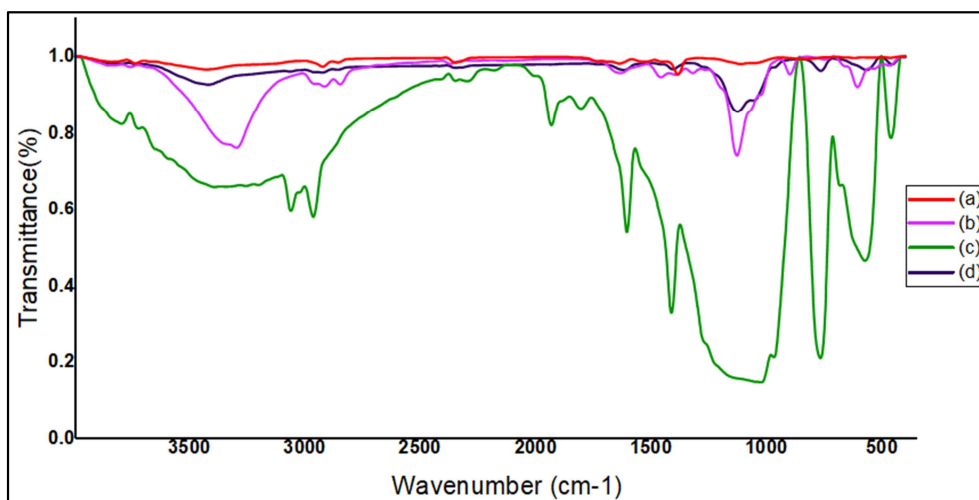
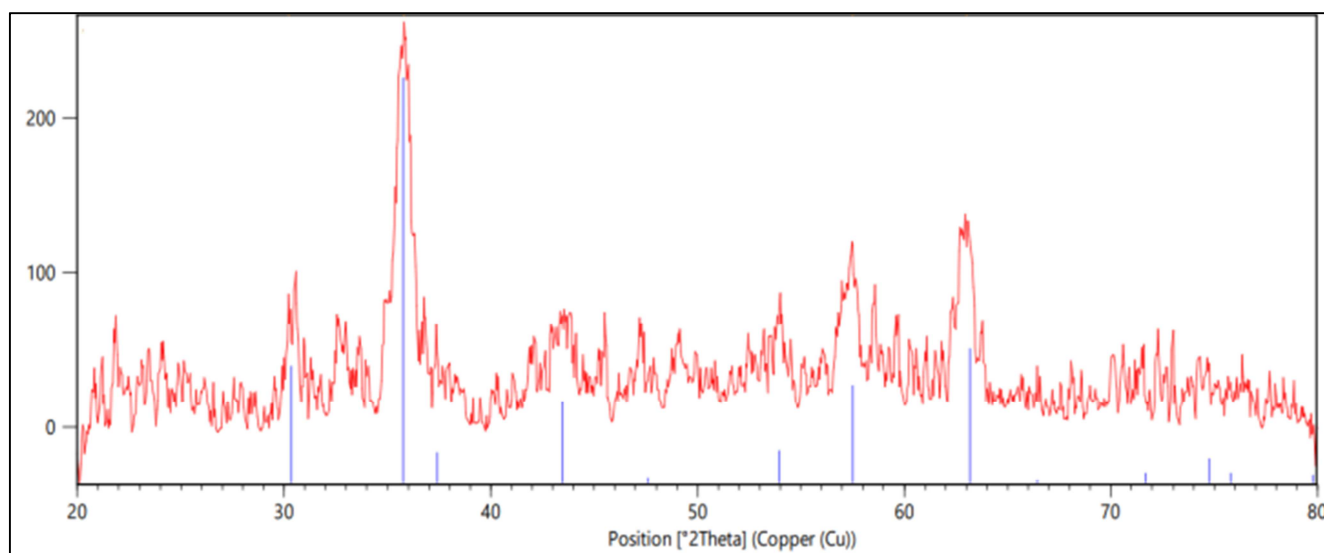
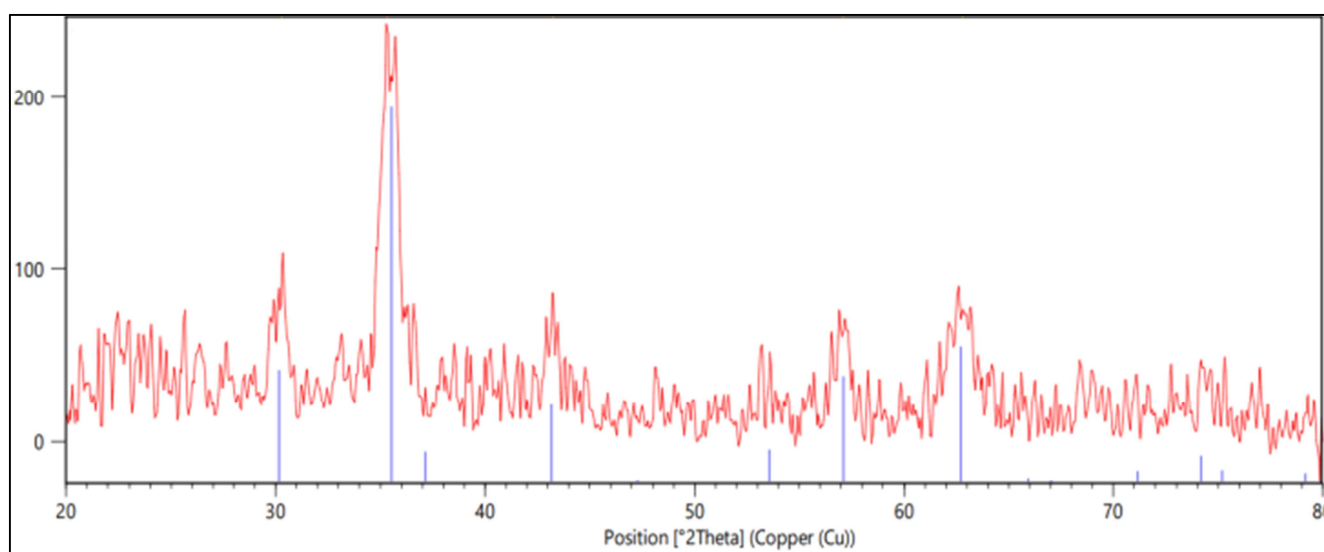


Figure 1. FT-IR spectra of Fe_3O_4 (a), $Fe_3O_4@SiO_2$ (b), $Fe_3O_4@SiO_2@VTES$ (c), and $MNPs@PIL$ (d).



a)



b)

Figure 2. XRD patterns of Fe_3O_4 (a) and $MNPs@PIL$ (b).

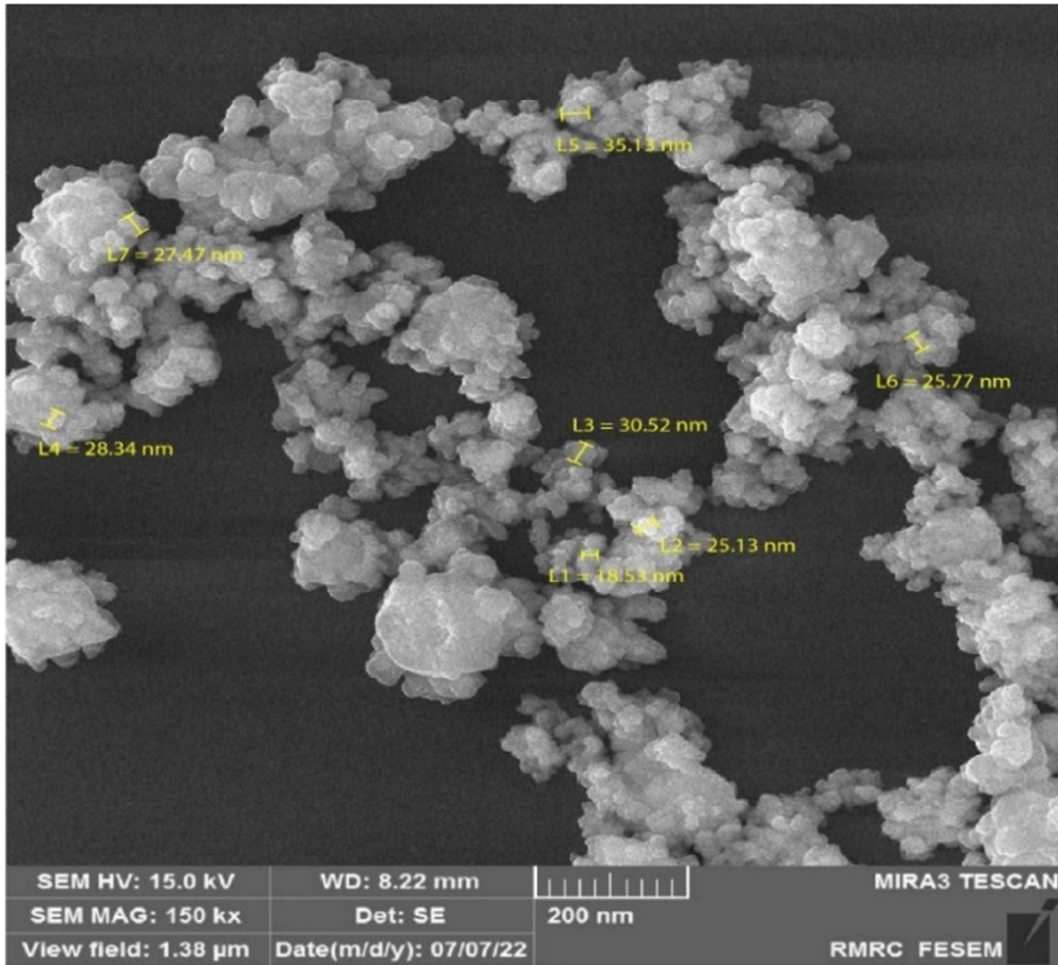


Figure 3. SEM image of MNPs@PIL.

3.1.4. Transmission Electron Microscopy (TEM)

In “Figure 4”, The morphology of the MNPs@PIL was examined using transmission electron microscopy (TEM). The obtained result confirmed the nanometer size of MNPs@PIL and also showed that the poly (ionic liquid) was placed as a thin layer on the absorbent surface.

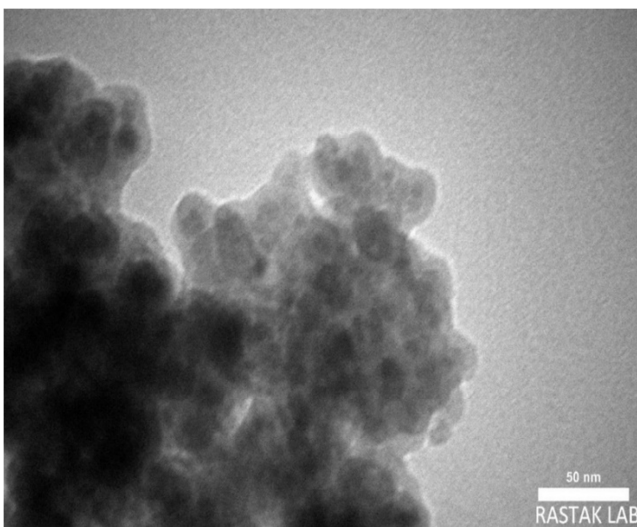


Figure 4. TEM image of MNPs@PIL.

3.2. Adsorption Process

3.2.1. The Effect of pH Value

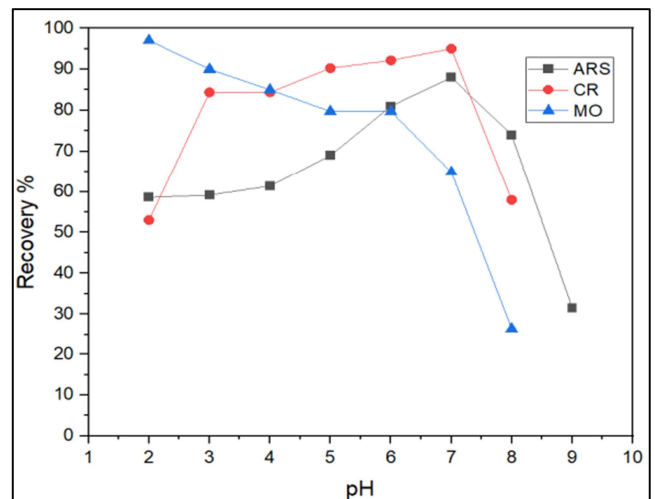


Figure 5. Effect of pH on the recovery of Alizarin Red S, Congo red and Methyl orange.

“Figure 5”, shows the effect of sample pH on extraction efficiency. The results showed that when the other conditions were constant, the pH value strongly affected the extraction

efficiency of MNPs because it can determine the surface charge of the adsorbent [19]. The pH range was evaluated from 2 to 9 for Methyl orange, Congo red, and Alizarin red S dyes. The extraction efficiencies for Congo red and alizarin red S dyes improved with the increase of pH (2-7) values and reached the maximum at pH value 7 (98%). Moreover, methyl orange dye has been optimized at pH=2 with 97% recovery. With the increase of sample pH values, a strong electrostatic attraction has been created between the OH⁻ groups and the adsorbent active groups. But at pH 8-9, due to the creation of electrostatic repulsion between the analyte molecules and the adsorbent surface, the extraction efficiency has decreased to 55.97, 24 and 26.41%, respectively.

3.2.2. The Effect of Extraction Time

The effect of extraction time on the extraction performance for anionic dyes was investigated. The extraction time varied from 5 to 17 min. As shown in “Figure 6”, Results indicated that the extraction performance increased from 5 to 15 min, the adsorption percentage of the dyes also increased, and after that, the adsorption efficiency remained almost constant at 17 min. Therefore, 15 min is considered the maximum adsorption time for all three dyes.

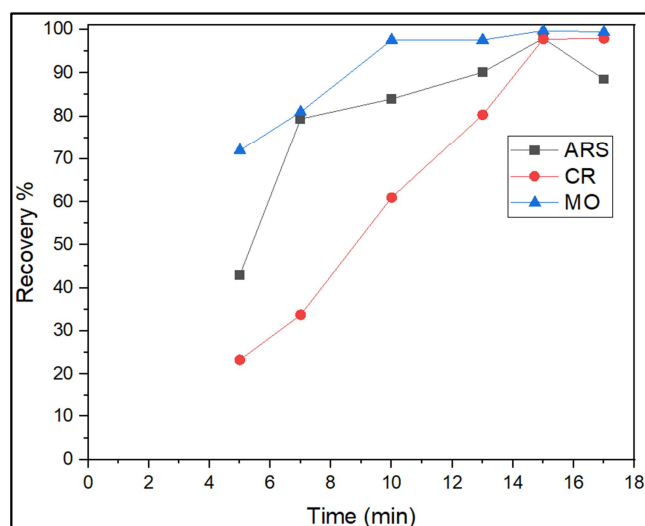


Figure 6. Effect of time on the recovery of Alizarin Red S, Congo red and Methyl orange.

3.2.3. Effect of the Amount of the Sorbent

In order to determine the optimum amount of adsorbent required for quantitative sorption of Methyl orange, Congo red, and Alizarin red S dyes, different quantities of *MNPs@PIL* were used in this step in the range of 40 to 100 mg. As shown in “Figure 7”, the highest extraction efficiency was obtained in the values of 80 mg adsorbent, 97, 97.8, and 98.82%, respectively. Consequently, the optimum amount of the adsorbent was 80 mg.

3.2.4. Effect of Temperature on Sample Adsorption

Temperature is one of the important factors that affects the adsorption process. In this study, the effect of temperature was investigated in the range of 5 to 30°C for the adsorption

of Methyl orange, Congo red, and Alizarin red S dyes. The obtained results are shown in “Figure 8”, and the highest extraction efficiency was calculated at 10°C for CR and 15°C for ARS and MO. As the temperature increases, the interaction between the dye molecules and the active sites of the adsorbent decreases. Therefore, the extraction efficiency will decrease.

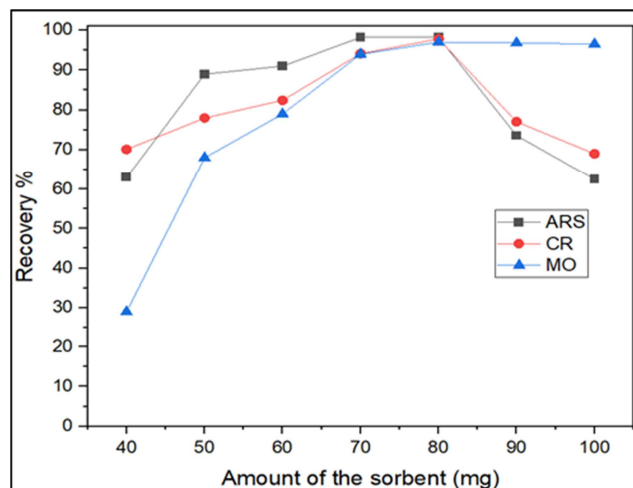


Figure 7. Effect of the Amount of the sorbent on the recovery of Alizarin Red S, Congo red and Methyl orange.

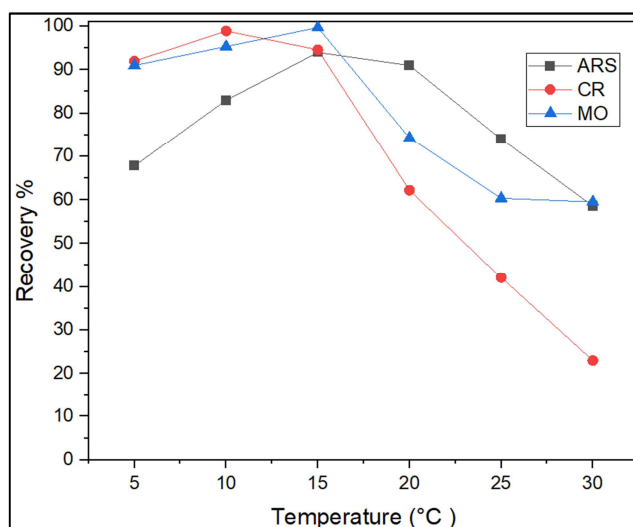


Figure 8. Effects of temperature on the recovery of Alizarin Red S, Congo red and Methyl orange.

3.2.5. Kinetic Model

To study the kinetics of dye adsorption onto *MNPs@PIL*, the kinetic investigations were performed for Mo, CR, and ARS dyes. The experimental data of the pseudo-first-order and pseudo-second-order adsorption kinetic models for the adsorption process of dyes by *MNPs@PIL* adsorbent was investigated.

The linear equation of the pseudo first order kinetic model is expressed as follows:

$$\ln(q_e - q_t) = \ln q_e - K_1 t \quad (1)$$

The pseudo-second-order kinetic equation is expressed as follows [20]:

$$t/q_e = 1/K_2q_e^2 + 1/q_e t \quad (2)$$

“In equation 1 and 2”, q_e (mg/g^{-1}), and q_t (mg/g^{-1}) mean the amount of dyes adsorbed on *MNPs@PIL* at equilibrium time, and t (min) is time, K_1 and k_2 are rate

constants of pseudo-first order and pseudo-second order kinetic model. Constant parameters and correlation coefficients (R^2) of these two models for dye adsorption by *MNPs@PIL* adsorbent are shown in “Table 1”. According to these results, pseudo-second-order kinetic model fits better the experimental data. so it can be concluded that the adsorption process follows the pseudo-second-order model.

Table 1. The kinetic parameters for the removal of MO, CR and ARS.

Dye	Pseudo-first-order			Pseudo-second-order		
	K_1	$q_e(mg/g^{-1})$	R^2	K_2	$q_e(mg/g^{-1})$	R^2
MO	1.3096	0.1948	0.943	0.7514	0.02271	0.9622
CR	0.98708	0.221	0.9279	0.7936	0.02843	0.9463
ARS	1.2795	0.2317	0.9371	0.6634	0.01940	0.96

3.2.6. Adsorption Isotherm

In order to find the adsorption mechanism of Mo, CR and ARS on the surface of *MNPs@PIL* adsorbent, Langmuir and Freundlich isotherm models were investigated. The Langmuir isotherm model is based on monolayer adsorption.

The equation of the Langmuir isotherm model can be written as follows [21]:

$$C_e/q_e = 1/q_m K_L + C_e/q_m \quad (3)$$

The Freundlich isotherm experimental model is based on multilayer adsorption on the absorbent surface. The linear form

of Freundlich model equation is expressed as follows [22]:

$$\ln(q_e) = \ln(K_f) + 1/n \ln(C_e) \quad (4)$$

“In equation 3 and 4”, q_e is the equilibrium adsorption capacity ($mg.g^{-1}$), q_{max} is the maximum adsorption capacity ($mg.g^{-1}$), K_L is the Langmuir adsorption equilibrium constant ($L.mg^{-1}$), K_f is the equilibrium adsorption coefficient ($L.mg^{-1}$), and $1/n$ is an empirical constant. The results obtained from adsorption isotherms (Table 2) demonstrated monolayer adsorption of MO, CR, and ARS onto *MNPs@PIL*.

Table 2. Fitted Langmuir and Freundlich isotherm parameters for adsorption of MO, CR and ARS onto *MNPs@PIL*.

Dye	Langmuir isotherm			Freundlich isotherm		
	$q_e(mg/g)$	$K_L(L/mg)$	R^2	$K_f(mg/g)$	$1/n$	R^2
MO	22.22	0.47	0.9875	0.333	0.7165	0.9006
CR	47.61	0.12	0.984	0.156	0.8553	0.9755
ARS	17.8	0.81	0.9894	0.290	1.3371	0.9651

3.3. Desorption Process

3.3.1. The Effect of Desorption Time

Desorption time was studied by varying the time from 5 to 30 min. The results are shown in “Figure 9”, it was found that as the time increased to 25 minutes, desorption efficiency for Mo, CR, and ARS dyes reaches 95.67, 96.10, and 96% respectively and after that, there was no change in the extraction efficiency.

3.3.2. Effect of Initial Dye Concentration and Loading Capacity

To determine the maximum volume of the sample solution and calculating preconcentration factor different volumes of sample solutions from 20 to 50 mL containing fixed amounts of 6.4, 7.7 and 8.35 micrograms methyl orange, Congo red and alizarin red S, respectively using sodium hydroxide solvent (0.2 M) and ethanol (0.5 - 0.7 M) were investigated. The results are shown in “Figure 10”, as can be seen, the recovery efficiency has decreased with the increase of the sample volume. The amount of washing solvent for all 3 dyes was 20 and 25 ml, and the preconcentration factor for methyl orange, Congo Red and Alizarin Red S was calculated as 4, 5

and 3.3, respectively.

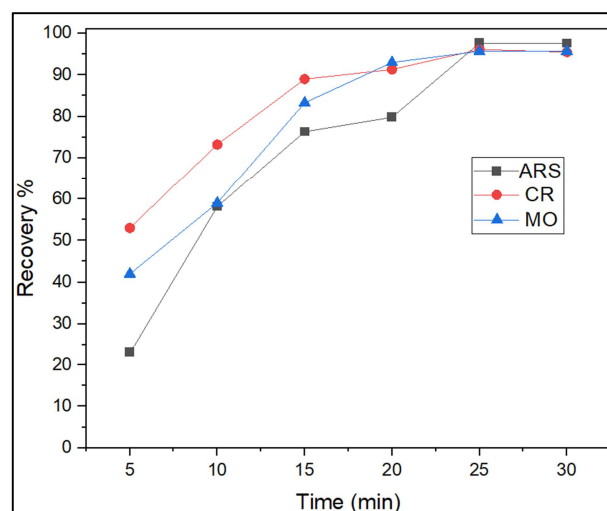


Figure 9. Effect of time on the recovery of the Alizarin Red S, Congo red and Methyl orange.

3.3.3. Analytical Performance

The limit of detection (LOD), the limit of quantification

(LOQ) and the correlation coefficient for methyl orange, Congo red, and alizarin red S dyes were investigated under the optimized conditions. The detection limit (LOD) was determined as 0.039, 0.096, and 0.043 ($\text{mg}\cdot\text{L}^{-1}$) for methyl orange, Congo red, and alizarin red S, respectively. The correlation coefficient (R^2) was determined to be 0.99 for all

3 dyes. The limit of quantification (LOQ) was 0.39, 0.96, and 0.43 ($\text{mg}\cdot\text{L}^{-1}$) for Methyl orange, Congo red, and Alizarin red S, respectively. Comparison of this method with other methods is presented in Table 3. The current method has a high performance compared to other methods.

Table 3. Comparison of analytical performance of this method with other methods for determining dyes MO, CR and ARS.

Adsorbent	Method	Dye	q_m (mg/g)	References
Chitosan-Silica Nanocomposite	UV-Vis	MO	7.0	[23]
Carbon Nanomaterials	UV	RAS	20	[24]
Activating natural bentonite	UV-Vis	CR	7.0	[25]
$\text{Fe}_3\text{O}_4@/\text{SiO}_2@/\text{PIL}$	MSPE-FL	CR	5.24	[26]
$\text{Fe}_3\text{O}_4@/\text{SiO}_2@/\text{PIL}$	UV-Vis	MO	18.08	This work
		CR	47.61	
		ARS	22.22	

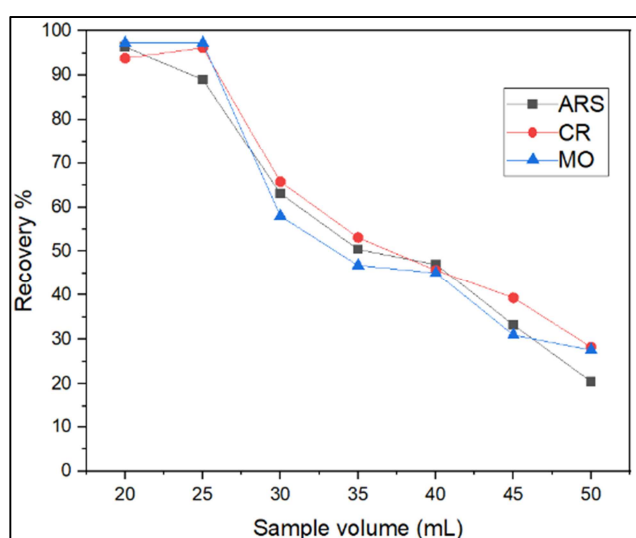


Figure 10. Effect of sample volume on the recovery of the Alizarin Red S, Congo red and Methyl orange.

3.3.4. Analysis of Real Water Samples

The proposed method was for measuring dyes in real water samples. tap water, river, lake, well water, and Dyeing effluent were examined. Before the test, all of the real samples were first filtered to remove impurities and after adjusting the pH of each sample, different amounts of dye were added to the water samples and filtered again by 0.45 micrometer membranes. Certain amounts of dyes were added to each real sample and all of the obtained optimum conditions were considered. Eluting solutions were evaluated using a UV-Vis spectrometer. Acceptable recoveries were obtained in the range from 80.61 to 104%. The results are shown in "Table 4".

Table 4. The recovery percentage of each analyte from real samples by adding a fixed amount of analyte to the sample.

Samples	Dye	Recovery %
Tap Water	MO	104
	CR	97.18
	ARS	96.19
	MO	92.73
River Water (Qazvin)	CR	90.99
	ARS	94.73

Samples	Dye	Recovery %
River Water (Gilan)	MO	81
	CR	88.74
	ARS	90.61
Well Water (Gilan)	MO	94.38
	CR	96.26
	ARS	93.19
Lake Water (Gilan)	MO	80.61
	CR	83.54
	ARS	86.21
Dyeing effluent (Buin Zahra)	MO	95.99
	CR	94.93
	ARS	99.77

4. Conclusion

In this research, the synthesis, properties and use of magnetic nanoparticles coated with polymer ionic liquid as new and efficient adsorbent for the separation and extraction of MO, CR and ARS anionic dyes in water samples were presented. Kinetic and isotherm studies demonstrated that pseudo-second-order kinetic and Langmuir isotherm models are followed. The obtained results and the comparison of this method with other methods of removing these dyes showed this method has enough efficiency. Also the proposed method has a good separation speed, the reason for that is the simplicity of the method, as well as the presence and polymerization of imidazolium groups on the surface of magnetic nanoparticles with high surface area which provides more active adsorption sites, so increases adsorption efficiency. The high extraction efficiency and low cost of this method are superior to other methods.

References

- Wu, L., Yu, L., Ding, X., Li, P., Dai, X., Chen, X., & Ding, J. (2017). Magnetic solid-phase extraction based on graphene oxide for the determination of lignans in sesame oil. *Food chemistry*, 217, 320-325.
- Herrero-Latorre, C., Barciela-García, J., García-Martín, S., Peña-Creciente, R. M., & Otárola-Jiménez, J. (2015). Magnetic solid-phase extraction using carbon nanotubes as sorbents: a review. *Analytica Chimica Acta*, 892, 10-26.

- [3] Deng, Y., Qi, D., Deng, C., Zhang, X., & Zhao, D. (2008). Superparamagnetic high-magnetization microspheres with an Fe₃O₄@ SiO₂ core and perpendicularly aligned mesoporous SiO₂ shell for removal of microcystins. *Journal of the American Chemical Society*, 130 (1), 28-29.
- [4] Ulman, Abraham. (1996) "Formation and structure of self-assembled monolayers." *Chemical reviews* 96.4, 1533-1554.
- [5] Pham, Thi Phuong Thuy, Chul-Woong Cho, and Yeoung-Sang Yun. (2010) "Environmental fate and toxicity of ionic liquids: a review." *Water research* 44.2, 352-372.
- [6] Yuan, Jiayin, & Markus Antonietti. (2011) "Poly (ionic liquid) s: Polymers expanding classical property profiles." *Polymer* 52.7, 1469-1482.
- [7] Yuan, Jiayin, David Mecerreyes, & Markus Antonietti. (2013) "Poly (ionic liquid) s: An update." *Progress in Polymer Science* 38.7, 1009-1036.
- [8] Young, Joshua A., Zhang, C., Devasurendra, A. M., Tillekeratne, L. V., Anderson, J. L., & Kirchhoff, J. R. (2016). Conductive polymeric ionic liquids for electroanalysis and solid-phase microextraction. *Analytica chimica acta*, 910, 45-52.
- [9] Devasurendra, A. M., Zhang, C., Young, J. A., Tillekeratne, L. V., Anderson, J. L., & Kirchhoff, J. R. (2017). Electropolymerized pyrrole-based conductive polymeric ionic liquids and their application for solid-phase microextraction. *ACS applied materials & interfaces*, 9 (29), 24955-24963.
- [10] Aflatouni, F., & Soleimani, M. (2018). Preparation of a new polymerized ionic Liquid-Modified magnetic nano adsorbent for the extraction and preconcentration of nitrate and nitrite anions from environmental water samples. *Chromatographia*, 81 (11), 1475-1486.
- [11] Huang, X., Chen, L., Yuan, D., & Bi, S. (2012). Preparation of a new polymeric ionic liquid-based monolith for stir cake sorptive extraction and its application in the extraction of inorganic anions. *Journal of Chromatography A*, 1248, 67-73.
- [12] Mohan, S. Venkata, N. Chandrasekhar Rao, & J. Karthikeyan. (2002) "Adsorptive removal of direct azo dye from aqueous phase onto coal-based sorbents: a kinetic and mechanistic study." *Journal of hazardous materials* 90.2, 189-204.
- [13] Modak, Jayant B., Avijit Bhowal, & Siddhartha Datta. (2016) "Extraction of dye from aqueous solution in rotating packed bed." *Journal of hazardous materials* 304, 337-342.
- [14] Bhowmik, M., Debnath, A., & Saha, B. (2020). Fabrication of mixed phase CaFe₂O₄ and MnFe₂O₄ magnetic nanocomposite for enhanced and rapid adsorption of methyl orange dye: statistical modeling by neural network and response surface methodology. *Journal of Dispersion Science and Technology*, 41 (13), 1937-1948.
- [15] Wu, Zhijian, Joo, H., Ahn, I. S., Haam, S., Kim, J. H., & Lee, K. (2004). Organic dye adsorption on mesoporous hybrid gels. *Chemical Engineering Journal*, 102 (3), 277-282.
- [16] Yang, Jia-Ying, Jiang, X. Y., Jiao, F. P., & Yu, J. G. (2018). The oxygen-rich pentaerythritol modified multi-walled carbon nanotube as an efficient adsorbent for aqueous removal of alizarin yellow R and alizarin red S. *Applied Surface Science*, 436, 198-206.
- [17] Gautam, Ravindra Kumar, Ackmez Mudhoo, & Mahesh Chandra Chattopadhyaya. (2013) "Kinetic, equilibrium, thermodynamic studies and spectroscopic analysis of Alizarin Red S removal by mustard husk." *Journal of Environmental Chemical Engineering* 1.4, 1283-1291.
- [18] Deng, Yonghui, Qi, D., Deng, C., Zhang, X., & Zhao, D. (2008). Superparamagnetic high-magnetization microspheres with an Fe₃O₄@ SiO₂ core and perpendicularly aligned mesoporous SiO₂ shell for removal of microcystins. *Journal of the American Chemical Society*, 130 (1), 28-29.
- [19] Asghar Nezhad, A. A., Mollazadeh, N., Ebrahimzadeh, H., Mirbabaei, F., & Shekari, N. (2014). Magnetic nanoparticles based dispersive micro-solid-phase extraction as a novel technique for coextraction of acidic and basic drugs from biological fluids and waste water. *Journal of Chromatography A*, 1338, 1-8.
- [20] Ho, Yuh-Shan, & Gordon McKay. (1998) "Sorption of dye from aqueous solution by peat." *Chemical engineering journal* 70.2, 115-124.
- [21] Yen, Ming-Tsung, Joan-Hwa Yang, & Jeng-Leun Mau. (2009). "Physicochemical characterization of chitin and chitosan from crab shells." *Carbohydrate polymers* 75.1, 15-21.
- [22] Kumar, M., Tamilarasan, R., & Sivakumar, V. (2013). Adsorption of Victoria blue by carbon/Ba/alginate beads: kinetics, thermodynamics and isotherm studies. *Carbohydrate polymers*, 98 (1), 505-513.
- [23] Mohammed, M. I., Ismael, M. K., & Gönen, M. (2020, February). Synthesis of Chitosan-Silica Nanocomposite for Removal of Methyl Orange from Water: Composite Characterization and Adsorption Performance. In *IOP Conference Series: Materials Science and Engineering* (Vol. 745, No. 1, p. 012084). IOP Publishing.
- [24] Ghaedi, M., Najibi, A., Hossainian, H., Shokrollahi, A., & Soylak, M. U. S. T. A. F. A. (2012). Kinetic and equilibrium study of Alizarin Red S removal by activated carbon. *Toxicological & environmental chemistry*, 94 (1), 40-48.
- [25] Toor, M., Jin, B., Dai, S., & Vimonses, V. (2015). Activating natural bentonite as a cost-effective adsorbent for removal of Congo-red in wastewater. *Journal of Industrial and Engineering Chemistry*, 21, 653-661.
- [26] Fan, L., Zhang, Y., Li, X., Luo, C., Lu, F., & Qiu, H. (2012). Removal of alizarin red from water environment using magnetic chitosan with Alizarin Red as imprinted molecules. *Colloids and Surfaces B: Biointerfaces*, 91, 250-257.